SUPPLEMENTARY METHODS

Strategies for microbial opsin expression in PV::Cre mice. The simplest approach for microbial opsin expression in PV::Cre mice takes advantage of a cassette consisting of three polyadenylation STOP signals flanked by two loxP sites in the same orientation (Supplementary Fig. 1a, top) that can be excised by Cre recombinase in those PV neurons that express Cre. This approach has been used for labeling PV neurons[1]. However, we and others have experienced that viral transduction with floxed-stop constructs results in a significant level of transcriptional leak without Cre (Supplementary Fig. 1b, top panels). To eliminate transcriptional leakiness, we devised several other strategies, including use of single- and double-floxed inverse open reading frames (Supplementary Fig. 1a, middle and bottom). Cre will reversibly invert rather than excise a DNA fragment flanked by two oppositely oriented lox sites[2], and if the transgene is initially oriented in the antisense orientation, transcriptional activity is unable to generate any opsin mRNA without Cre. While this single-floxed inverted construct indeed exhibited no transcriptional leakiness in the absence of Cre, opsin expression level in Cre-cotransfected cells was weak (Supplementary Fig. 1b, middle panels), likely due to the transgene undergoing continuous inversion.

Construction of Cre-activated recombinant AAV vectors. Because of the issues described above, double-floxed inverted constructs (Fig. 1a; Supplementary Fig. 4) provide a preferable strategy, in which two nested pairs of incompatible lox sites are used[3,4], loxP and lox2722. In Cre-expressing cells, ChR2 or eNpHR is first reversibly flipped into the sense orientation via either pair of sites (Fig. 1b); this first reversible step enables a second irreversible excision event that prevents further inversion (Fig. 1b). The DNA cassette carrying two pairs of incompatible

lox sites (loxP and lox2722) was synthesized (DNA2.0, Menlo Park, CA) and the ChR2-EYFP transgene was inserted between the loxP and lox2722 sites (Fig. 4) in the reverse orientation. The resulting double-floxed reverse ChR2-EYFP cassette was cloned into a modified version of the pAAV2-MCS vector (Stratagene, La Jolla, CA) carrying the EF-1a promoter and the Woodchuck hepatitis virus posttranscriptional regulatory element (WPRE) to enhance expression. For a detailed description of the vector system see Supplementary Fig. 4. The recombinant AAV vectors were serotyped with AAV5 coat proteins and packaged by the viral vector core at the University of North Carolina. The final viral concentration was 2×10^{12} genome copies / mL.

Stereotactic injection. Doublefloxed reversed ChR2-EYFP or eNpHR-EYFP virus was injected stereotactically into 5-6 week-old PV::Cre mice. Injections were carried out under isoflurane anesthesia. 0.5 µl virus was injected into infralimbic pre-frontal cortex (anteroposterior, 1.7mm; mediolateral, 0.4mm; dorsoventral 2.5mm) using a microsyringe pump (World Precision Instruments). Experiments were carried out at least 2 weeks later to allow for viral expression.

***In vivo* optrode recording**: Simultaneous optical stimulation and electrical recording in the infralimbic and prelimbic cortices of PV::Cre transgenic mice transduced with double-floxed AAV:eNpHR-EYFP and ChR2-EYFP (under control of the CaMKII promoter) was carried out as described previously[5] using an optrode consisting of an extracellular tungsten electrode (1 MΩ, ~125 µm, A.M Systems) tightly bundled with an optical fiber (200 µm core diameter, 0.2 N.A., ThorLabs), with the tip of the electrode protruding slightly beyond the fiber end (~0.4 mm) to ensure illumination of the recorded neurons. Recordings were conducted with the optrode initially placed at the top of prelimbic (PL) cortex (from bregma: anterior-posterior, -1.8mm;

lateral, 0.3mm; and dorsal-ventral, 2.0mm) and gradually lowered in 0.1 mm increments towards infralimbic (IL) cortex. The electride-coupled optical fiber was coupled to 473 nm and 589 nm solid-state laser diodes (LaserGlow Technologies). The light from the two laser diodes were joined via a visible-wavelength Y fiber splitter (Fiber Optic Network Technology, Co.) The 473 nm and 589 nm laser diodes were adjusted to have an output of 20 and 35 mW respectively. Local field potential recordings were done in mice anesthetized with a ketamine/xylazine mixture. Signals were recorded and band-pass filtered at 1 Hz low/5 kHz high using an 1800 Microelectrode AC Amplifier (A-M Systems). The pattern of blue light flashes was based on a 14 second long multiunit recording from medial prefrontal cortex (mPFC) in an freely moving awake rat, in which the mean firing rate was 20.1 Hz. Blue light flashes were 5 msec in duration, and we only analyzed flashes that were separated from other flashes by at least 25 msec (175 / 282 flashes satisfied this criterion).

***In vitro* electrophysiology.** Patch clamp recordings in brain slices and dynamic clamp were carried out as previously described[6].

Slice preparation: Experiments were performed in accordance with procedures established by the Administrative Panel on Laboratory Animal Care at Stanford University. For dynamic clamp experiments, we cut 225 micron horizontal slices from postnatal day 21-35 C57Bl/6 mice. For optogenetic stimulation of prefrontal pyramidal neurons we cut 300 micron horizontal or coronal slices from 6-10 week old transgenic mice expressing ChR2 under the control of the Thy1 promoter. To study fast-spiking interneurons in prefrontal cortex, we cut 300 micron coronal slices from 6-10 week old transgenic mice which express Cre recombinase under control of the parvalbumin promoter, and had undergone stereotactic injection of lentivirus carrying DIO

EYFP-ChR2. Slices were prepared in a chilled sucrose solution, then incubated in ACSF at 30.5°C for 1 hr prior to recording.

Intracellular Recording: To study the effects of oscillations on sEPSC-spike rate information using dynamic clamp, we made whole cell patch recordings from visually identified pyramidal cells in deep layer V or layer VI of frontal cortex. For experiments using optogenetic stimulation of prefrontal pyramidal neurons, we recorded from visually identified pyramidal neurons or interneurons in layer V of mPFC. To study the role of fast-spiking interneurons in prefrontal cortex, we recorded from either layer II/III or layer V pyramidal neurons in regions of mPFC containing EYFP expressing neurons. Of note, in these experiments we did not block excitatory synaptic transmission, simply because spontaneous EPSCs occur at a high rate in fast-spiking neurons and may thus contribute to their excitability. We used dynamic clamp to stimulate only a single pyramidal neuron, and it is exceedingly rare for single action potentials in PY neurons to recruit feedback inhibition from fast-spiking PV interneurons[7]. Recordings were made using a Multiclamp 700A (Axon Instruments). Patch electrodes (tip resistance = 2–6 MOhms) were filled with (in mM): 130 K-gluconate, 10 KCl, 10 Hepes, 10 EGTA, and 2 MgCl (pH adjusted to 7.3 with KOH) and ACSF contained (in mM): 126 NaCl, 26 $NaHCO_3$, 2.5 KCl, 1.25 NaH_2PO_4, 1 $MgCl_2$, 2 CaCl, and 10 glucose. All recordings were at 32.5 ± 1 °C. Series resistance was usually 10–20 M, and experiments were discontinued if it exceeded 30 M. The membrane potential was corrected for a measured liquid junction potential of 7 mV.

Dynamic clamp: We implemented dynamic clamp using custom-written software running under the Real Time Application Interface for Linux (RTAI). Output currents updated at 10 KHz. Bridge balance was adjusted throughout experiments. Unless otherwise noted, sEPSCs had peak conductances of 4 nS, decayed with a time constant of 2 msec, and reversed at 0 mV. When

feedback inhibition was implemented via dynamic clamp, it consisted of a monoexponentially decaying conductance with variable peak conductances and time constants of decay (Supplementary Tables 1, 2), reversed at -60 mV, and occurred 2.5 msec after each PY neuron spike.

ChR2 / eNpHR stimulation *in vitro:* We stimulated ChR2 in pyramidal neurons using flashes of light lasting 1 msec, generated by a Lambda DG-4 high speed optical switch with a 300W Xenon lamp, and a GFP filter set (excitation filter HQ470/40x, dichroic Q495LP; Chroma), delivered to the slice through a 40x objective (Olympus). We used light flashes lasting 5 msec to stimulate ChR2 in fast-spiking interneurons. We stimulated eNpHR in fast-spiking interneurons *in vitro* using continuous yellow light generated in similar fashion, using a Lambda DG-4 and a 593 nm filter set, again delivered through a 40x objective (Olympus). Illumination was delivered across a full high-power (40x) field.

Estimated numbers of neurons activated by light stimulation *in vitro***.** Illumination was delivered across a full high-power (40x) field, and we found that if we recorded from a cell at the center of a high power field, and shifted the illumination one high-power field in either direction, then the light-activation was lost. Therefore, we actually activated relatively small subsets of target neurons, whether. PY neurons in Thy1 transgenic mice or PV interneurons in virus-injected PV::Cre mice. Given that a high power field (40x, hpf) is approximately 260 microns in diameter, there should be ~80 neurons/hpf, ~60% and 10% of which are PY and PV cells, respectively. Thus, we estimate there are ~48 PY and 8 PV neurons / hpf. In slices from Thy1 transgenic mice, we found that >50% of the PY cells we patched expressed ChR2, while approximately 25-50% of PV interneurons were fluorescent in virus-injected PV::Cre mice. Thus, we expect each light flash to activate approximately 24-48 PY neurons in slices from Thy1

transgenic mice, and 2-4 PV interneurons in slices from virus-injected PV::Cre mice. The latter figure is consistent with the numbers of fluorescent cells / hpf we observed while recording from virus-injected PV::Cre mice. An EPSC from one pyramidal neuron to one interneuron has an amplitude ~ 100 pA and τ_{decay} ~ 10 msec at room temperature (Wantanabe, 2005), i.e. τ_{decay} ~ 3-5 msec at 32-34 °C. Light flashes in virus-injected PV::Cre mice evoked currents ~ 200-300 pA in fast-spiking interneurons (Supplementary Fig. 1e). Since we used 5 msec long flashes, the total charge would be ~ 250 pA x 5 msec ~ 1250 nC, which is approximately equal to the total charge from 3 unitary pyramidal neuron – interneuron connections. In addition, Fig. 2b shows a high-frequency train of blue light flashes to activate ChR2-expressing PV interneurons, shunts responses to current injection in a PY neuron with R_{in} ~ 100-200 MΩ by ~ 50%, suggesting that this strategy recruits a maximal inhibitory conductance around 5-10 nS.

Design of sEPSC and light pulse trains: sEPSC trains used to measure sEPSC-spike rate information were generated as follows. Each experiment was divided into sweeps that were 5 or 10 seconds long and separated by 2.5-5 seconds to minimize rundown. Each sweep was subdivided into 500 msec segments. The total number of sEPSCs during each 500 msec segment was between 0 and 250. This sequence of sEPSC rates was the same for rhythmic and non-rhythmic trains. Then, the times of sEPSCs were randomly selected from a uniform distribution extending across either the entire 500 msec segment (for non-rhythmic trains) or across half the time window corresponding to the ON period of the oscillation (for rhythmic trains), i.e. half of each 25 or 125 msec cycle for 8 or 40 Hz modulation, respectively. Light pulse trains were constructed in similar fashion, using light pulse rates between 5 and 50 Hz, and sweeps that lasted 5 seconds and were separated by 10 seconds. This arrangement was motivated by the following observations: First, in the hippocampus, pyramidal neuron firing rates are the same

during non-rhythmic epochs and when theta oscillations occur[8]. As a result, spikes are concentrated more tightly near the peak of the oscillation (and more spread out during the trough), but the total number of events / cycle is the same in rhythmic and non-rhythmic cases, exactly as we have assumed. Second, suppose N input neurons synapse onto the pyramidal cell of interest, and each input neuron fires R spikes / sec. Suppose that each of these inputs is oscillating at 40 Hz, i.e. the spikes occur near the peak of the oscillation. Now consider two cases. If the N neurons are not synchronized, then in each gamma cycle, there are (N*R / 40) EPSCs, distributed across the cycle (non-rhythmic case). But if the input neurons are synchronized (rhythmic case), then in each gamma cycle there are the same number of EPSCs, all occurring near the peak of the oscillation. Note that in order to test the ability of feedback inhibition from PV interneurons to generate gamma rhythmicity in post-synaptic pyramidal neurons (Fig. 2), it was crucial to (1) adequately drive PV interneurons based on spiking from a single PY neuron, and (2) detect gamma rhythmicity in output spike trains from single PY neurons. For this reason, the experiments depicted in Fig. 2 utilized stronger levels of excitatory drive (i.e. sEPSCs with a unitary conductance = 8 nS, occurring at 1000 Hz).

Immunohistochemistry. To determine the specificity of ChR2-EYFP expression in PV neurons, PV::Cre mice transduced with the double-floxed AAV:ChR2-EYFP virus were anesthetized with ketamine/xylazine and perfused transcardially with phosphate-buffered saline (PBS, pH 7.4) followed by 4% paraformaldehyde (PFA) dissolved in PBS. The brains were removed and post-fixed in PBS containing 4% PFA overnight at 4 °C and subsequently immersed in a cryoprotectant consisting of PBS containing 30% sucrose until the brains settled (~48 hr at 4 °C). 45 μm coronal brain sections were collected and washed in PBS, treated with 0.3% Triton X-100

(PBST), and immersed in a blocking solution consisting of 3% normal donkey serum dissolved in PBS. Localization of PV cell bodies was confirmed by labeling with monoclonal anti-parvalbumin antibody (1:500; Sigma P3088). The staining procedure was same as described previously[9].

Measuring information in output spike trains. Quantifying the net effect of rhythmic modulation on information processing depends upon additional tools beyond I-O curve, maximum gain, and response variability alone. For example, the I-O curve in Fig. 3b suggests that the neuron's output is more informative about non-rhythmic inputs than theta-modulated inputs, because the difference between output spike rates in response to high and low input sEPSC rates is greater for non-rhythmic input than for theta-modulated input. However this effect may counteracted by decreased response variability in the case of theta-frequency case input. One solution would be to compute the cross-correlation between the input sEPSC rate and output spike rate, and indeed, both theta and gamma oscillations increase the cross-correlation. However, cross correlation is problematic because for very small window sizes (e.g. 10-15 msec), most windows contain zero spikes, so increases in cross-correlation often result from the output signal becoming more flat, rather than more informative. Conversely, for large windows (e.g. > 100 msec), there is a ceiling effect, and the response variability decreases relative to the range of possible responses, so that for all conditions, the correlation is near 1. To address these issues, we calculated mutual information (I_M), using the general formula:

$$I_M = \sum_{i,j} p(x_i, y_j) \log_2 \frac{p(x_i, y_j)}{p(x_i)p(y_j)}$$

where x_i represents possible values for one variable (e.g., the rate of input sEPSCs), y_j represents possible values for the second variable (e.g., the number of output spikes), and $p(x_i,y_i)$ represents the joint probability (the probability of observing y_j spikes and x_i sEPSCs). Note that the maximum information neural responses can transmit about their stimulus is the entropy of the stimulus set. Mutual information equals the difference between response entropy and noise entropy where response entropy is defined as:

$$H_{response} = -\sum_{j} p(y_j)\log_2 p(y_j)$$

And noise entropy is defined as:

$$H_{noise} = -\sum_{i,j} p(x_i)p(y_j|x_i)\log_2 p(y_j|x_i)$$

For example, we found that theta and gamma-frequency modulation sEPSC trains increased sEPSC-spike rate information, and this effect was attributable to decreased noise entropy (e.g. noise entropies for 125 msec window: non-rhythmic: 1.17±0.08 bits, γ: 0.93±0.06 bits; θ: 0.78±0.05 bits; $p<0.001$).

Mutual information calculated from undersampled probability distributions can be biased upwards, therefore all calculations of mutual information, response entropy, noise entropy, etc., were corrected for bias due to undersampling by computing values using smaller fractions (from one-half to one-eighth) of the data and extrapolating to the limit of infinite data[10, 11]. For sEPSC-spike rate information, the correction factors were typically ~ 1-2% and always < 5%. Using 25 msec windows to calculate information between pooled PY neuron activity and the responses of either FS interneurons or RS neurons the correction factors were ≤ 1%. Using 125 msec windows, the correction factors were < 10% for FS interneurons and < 15% for RS neurons.

Dynamic clamp experiments*:* to calculate sEPSC-spike rate information using windows of various sizes, the number of sEPSCs per window were divided into 10 equally spaced bins (corresponding to a stimulus entropy of 3.3 bits).

Using pooled activity from PY neurons in different slices to approximate the output from PY neurons to each FS interneuron (or RS neuron). Note that PY neurons in different slices produced very similar responses to the same train of light flashes, as measured by the cross-correlation between spike trains (0.75±0.02, n=66 cell pairs; no significant cross-slice correlation differences were observed between rhythmic and non-rhythmic light trains, p=0.26 by two-way ANOVA). This measure of the similarity of spike train responses across slices was even comparable to the cross-correlation between responses of the same neuron to repeated presentations of the same train of light flashes (0.89±0.02; n=12 cells). Because the responses of individual PY neurons in different slices are so similar (Fig. 4d), the temporal profile of pooled activity from many PY neurons responding to same light pulse train should be virtually identical in different slices (although differences in slice condition may affect the amplitude of synaptic output). Thus, we can accurately estimate the temporal profile of synaptic output from PY neurons across slices using the pooled activity of PY neurons recorded in response to light pulse trains.

ChR2 experiments*:* To calculate mutual information between pooled PY neuron activity and the response of an FS interneuron or RS neuron, x_i was the mean number of spikes produced by PY neurons during a 25 or 125 msec window, while y_j was the number of spikes in the FS interneuron or RS neuron during the same window. To divide pooled PY neuron activity into bins suitable for calculating I_M, we rounded the mean number of PY spikes within each time window to the nearest integer. Because the same number of light flashes could elicit different

numbers of PY neuron spikes, depending on whether the flashes occurred non-rhythmically, in a theta-frequency pattern, or in a gamma-frequency pattern, we used the same set of stimuli (i.e., the same range of PY neuron firing rates) to compare non-rhythmic and rhythmic stimuli. We also assumed a uniform prior, i.e. each stimulus occurred with equal probability. For calculations using 125-msec windows, the stimulus entropy was $\log_2(6) = 2.6$ bits for comparisons between non-rhythmic and gamma frequency light trains, and $\log_2(5) = 2.3$ bits for comparisons between non-rhythmic and theta frequency light trains. Because light stimulation rarely elicited PY neuron firing at rates above 50 Hz, to calculate information using 25 msec windows, we rounded the mean PY firing rate to 0 or 1 spike, corresponding to a stimulus entropy of 1 bit.

Calculating response variability. We defined the response variability as the standard deviation of the response to each sEPSC rate, normalized by the mean response of that neuron under all conditions (i.e. all input rates in non-rhythmic and rhythmic sEPSC trains), and averaged across all input rates.

Wavelet analysis. To compute the power spectra of spike trains**,** we convolved each spike train, $s(t)$, with wavelets of varying frequencies, i.e.:

$$W(f,t) = s(t) * g(f,t)$$

$$g(f,t) = e^{-t^2/2\sigma^2} e^{-2\pi i f t}$$

where * denotes convolution, $\sigma = 5/(6f)$, and spike trains were computed using 5 msec bins. We then used the squared amplitude of $W(f,t)$ over a 500 msec window to measure the power at various frequencies. Note that using this measure, isolated spikes will give rise to power across

frequencies. Simply normalizing the amplitude of $W(f,t)$ by the number of spikes would overcompensate for this effect. Thus, when comparing different spike trains, it is important to use approximately the same number of spikes in each case. Therefore, when comparing spike trains in the presence or absence of feedback inhibition, we randomly eliminated spikes from one spike train so that both trains contained equal numbers of spikes.

We computed the power spectra of local field potentials (LFPs) using the same wavelet functions $W(f,t)$. We used segments of the recorded LFP beginning 1 msec after the end of a light flash. To compute power at frequency f, we first band pass filtered the LFP between $f \pm 5$ Hz, then convolved with $W(f,t)$. After convolving, we obtained an amplitude and phase for each response. To measure phase locking, we converted each phase to a unit vector in the complex plane, averaged across all vectors from a single recording, and measured the amplitude (or absolute value) of the resulting averaged vector.

Classification of neurons during intracellular recording *in vitro*. We did not attempt an exhaustive classification of neuronal subtypes, but rather sought to (1) differentiate fast-spiking interneurons from other cell types, and (2) distinguish cells that were directly activated by light from those that were primarily activated indirectly, via synaptic excitation.

FS interneurons. Fast-spiking interneurons were readily identified by their narrow action potentials (half width = 0.30 ± 0.03 msec, n = 8 cells) and steep f-I slopes (0.81 ± 0.12 Hz/pA, n = 8 cells)[12]. The distributions of action potential half-widths (0.22 – 0.43 msec) and f-I slopes (0.38 – 1.4 Hz/pA) in fast-spiking interneurons were both completely non-overlapping with those of other cells (action potential half widths: 0.63 – 1.2 msec; f-I slopes: 0.14 - 0.36 Hz/pA). Fast-spiking interneurons had a round, multipolar appearance and relatively low input resistance (142

± 19 MΩ, n = 8 cells). The resting membrane potential was -77 ± 2 mV, after correcting for a liquid junction potential of 7 mV. During current clamp recording from fast-spiking interneurons, we frequently observed spontaneous EPSPs.

We determined whether responses to light flashes in a particular neuron were mediated mainly by direct activation of ChR2 or indirect synaptic excitation using the size and latency of light responses recorded in voltage clamp (at the resting membrane potential). For each cell, we used an automated algorithm to measure the latency between light flashes and the onset of responses in voltage clamp. In a subset of cells (12/29), we measured these voltage-clamp responses to light flashes after blocking excitatory synaptic transmission with CNQX (10-20 μM) and AP5 (50 μM). In every case, CNQX and AP5 blocked responses with a latency > 1.6 msec, whereas responses with latency < 1.6 were unaffected. Thus, short-latency (< 1.6 msec) responses represent direct activation of ChR2 by light, whereas longer-latency (> 1.6 msec) responses represent indirect responses mediated by synaptic excitation.

PY neurons. Using this approach, non fast-spiking cells fell into two non-overlapping groups. In the first group (n = 12 cells), light flashes elicited robust short-latency responses (mean slope = 601 pA/msec, range = 107 – 1808 pA/msec), and cellular responses followed 100 Hz stimulation. Neurons in this group had the morphology and electrophysiological properties of pyramidal neurons, e.g. wide action potentials (half width = 0.85 ± 0.04 msec), adapting responses to depolarizing current pulses, a relatively low input resistance (169 ± 14 MΩ) and high membrane capacitance (157 ± 18 pF). The resting membrane potential was -73 ± 2 mV, after correcting for a liquid junction potential of 7 mV. CNQX and AP5 did not abolish light-evoked responses in this group, as shown in Fig. 2b1 (n = 4 cells). In light of these observations and the knowledge that in this mouse line, the Thy1 promoter drives neocortical ChR2

expression primarily in layer V pyramidal neurons, we presumed this group represented pyramidal neurons expressing ChR2 that were directly activated by light.

RS neurons. In the second group (n = 9), light flashes evoked short-latency (< 1.6 msec) responses that were very weak or non-existent (mean slope = 5 pA/msec, range = 0-23 pA/msec), and cellular responses could never follow light stimulation at 100 Hz. In this group, CNQX and AP5 always abolished light-evoked responses (n = 4 cells). In each of these cells, indirect, i.e. long latency, responses evoked by light were at least an order of magnitude larger than the short-latency responses (mean slope of long latency responses = 284 pA/msec, range = 62-630 pA/msec). These neurons had diverse morphologies, adapting responses to depolarizing current pulses, and wide action potentials (half width = 0.79 ± 0.03 msec, n = 9 cells). Notably, although we identified this group using responses to light flashes as described above, compared to the presumptive pyramidal neurons, neurons in this group had significantly higher membrane resistance (418 ± 62 MΩ, $p < 0.001$ by two-tailed t-test) and lower membrane capacitance (75 ± 16 pF, $p < 0.01$ by two-tailed t-test). The resting membrane potential was -72 ± 3 mV, after correcting for a liquid junction potential of 7 mV. We assume that this group represents a heterogeneous group of non-fast-spiking neurons that are activated by light very weakly or not at all. Thus, this "regular spiking" group likely includes regular-spiking and adapting interneurons, as well as a few pyramidal neurons which do not express ChR2.

Using this approach, only 1/8 fast-spiking interneurons had appreciable direct activation by light. In the remaining 7/8 fast-spiking interneurons, short-latency (< 1.6 msec) responses were very weak or non-existent (mean slope = 3 pA/msec, range = 0-9 pA/msec) and at least 100-fold smaller than longer-latency (> 1.6 msec) responses (mean slope = 756 pA/msec, range = 148-2009 pA/msec). We applied CNQX and AP5 in 3 of these neurons, and found that they

completely blocked responses to light. Thus, we presume that in these 7/8 fast-spiking interneurons, responses to light were mediated almost entirely by indirect synaptic excitation, and therefore, we restricted analysis to these cells.

Notably, the finding that gamma oscillations increase information flow in FS interneurons but not in RS neurons may be explained in part by the observation that in FS interneurons, recovery from synaptic depression occurs on the same timescale as a gamma cycle[13].

Stability requirements for *in vitro* experiments. We only included data from recordings that were stable throughout an experiment, i.e. action potentials remained overshooting and the number of spikes evoked by repeated presentation of same sEPSC or light train changed by < 30%.

Integrate-and-fire simulations. We simulated the responses of 10 integrate-and-fire neurons to each of the non-rhythmic and rhythmic sEPSC trains used in dynamic clamp experiments using a timestep of 0.1 msec. Integrate-and-fire neurons had a membrane time constant of 15 msec. Input resistances were drawn from a uniform distribution between 180 and 220 MΩ, and spiking thresholds were drawn from a uniform distribution between 18 and 22 mV above the resting membrane potential. Spikes were followed by a reset of the membrane potential to the resting potential and an absolute refractory period of 5 msec. sEPSCs had a reversal potential 60 mV above rest, unitary conductance of 4 nS, and a decay time constant of 2 msec.

Biophysical simulations. We also simulated the responses of 10 single compartment model pyramidal neurons to each of the non-rhythmic and rhythmic sEPSC trains used in dynamic clamp experiments using a timestep of 0.02 msec. Model neurons had membrane capacitance of 75 pF (corresponding to a time constant of 15 msec for R_{in} = 200 MΩ). Input resistances were drawn from a uniform distribution between 180 and 220 MΩ, and resting membrane potentials were drawn from a uniform distribution spanning 4 mV. sEPSCs had a reversal potential 60 mV above rest, unitary conductance of 4 nS, and a decay time constant of 2 msec. Model neurons contained Hodgkin-Huxley type Na^+ and K^+ currents based on those of Traub and Miles[14], i.e. I_{Na} follows an m^3h formalism, I_K follows an n^4 formalism, and m, n, and h all have forward and reverse rates α and β, respectively, where:

$$\alpha_m = \frac{0.32(13-\bar{v})}{e^{(13-\bar{v})/4}-1}$$

$$\beta_m = \frac{0.28(\bar{v}-40)}{e^{(\bar{v}-40)/5}-1}$$

$$\alpha_h = 0.128e^{\frac{(17-\bar{v})}{18}}$$

$$\beta_h = \frac{4}{1+e^{(40-\bar{v})/5}}$$

$$\alpha_n = \frac{0.32(15-\bar{v})}{e^{(15-\bar{v})/5}-1}$$

$$\beta_n = 0.5e^{\frac{(10-\bar{v})}{40}}$$

Where $\bar{v} = v - v_{adj}$, v represents the membrane potential, and v_{adj} was -10 mV. g_{Na} was 0.25 or 1 μS as shown in Supplementary Fig. 8, and g_K was 0.125 or 0.5 μS in each of these two cases.

In addition to the results shown in Supplementary Fig. 8, we also simulated model neurons with g_{Na} between 0.25 and 5 μS, g_{Na}:g_K between 0.1 and 0.5, and v_{adj} between -20 and -5 mV.

REFERENCES

1. Kuhlman, S.J. & Huang, Z.J. High-resolution labeling and functional manipulation of specific neuron types in mouse brain by Cre-activated viral gene expression. *PLoS ONE* 3, e2005 (2008).
2. Sauer, B. Inducible gene targeting in mice using the Cre/lox system. *Methods (San Diego, Calif* 14, 381-392 (1998).
3. Zhang, F. Fast optical neural circuit interrogation technology: development and applications. *Larry Katz Memorial Lecture,* describing design and testing of single and doublefloxed inverted open reading frame strategies, *Cold Spring Harbor Laboratory Meeting on Neuronal Circuits: From Structure to Function* (March 13-16, 2008).
4. Atasoy, D., Aponte, Y., Su, H.H. & Sternson, S.M. A FLEX switch targets Channelrhodopsin-2 to multiple cell types for imaging and long-range circuit mapping. *J Neurosci* 28, 7025-7030 (2008).
5. Gradinaru, V.*, et al.* Targeting and readout strategies for fast optical neural control in vitro and in vivo. *J Neurosci* 27, 14231-14238 (2007).
6. Sohal, V.S. & Huguenard, J.R. Inhibitory coupling specifically generates emergent gamma oscillations in diverse cell types. *Proceedings of the National Academy of Sciences of the U.S.A.* 102, 18638-18643 (2005).
7. Silberberg, G. & Markram, H. Disynaptic inhibition between neocortical pyramidal cells mediated by Martinotti cells. *Neuron* 53, 735-746 (2007).
8. Klausberger, T.*, et al.* Brain-state- and cell-type-specific firing of hippocampal interneurons in vivo. *Nature* 421, 844-848 (2003).
9. Aravanis, A.M.*, et al.* An optical neural interface: in vivo control of rodent motor cortex with integrated fiberoptic and optogenetic technology. *J Neural Eng* 4, S143-156 (2007).
10. Strong, S.P., Koberle, R., de Ruyter van Steveninck, R.R. & Bialek, W. Entropy and information in neural spike trains. *Phys Rev Lett* 80, 197-200 (1998).
11. Gollisch, T. & Meister, M. Rapid neural coding in the retina with relative spike latencies. *Science* 319, 1108-1111 (2008).
12. Bacci, A., Rudolph, U., Huguenard, J.R. & Prince, D.A. Major differences in inhibitory synaptic transmission onto two neocortical interneuron subclasses. *J Neurosci* 23, 9664-9674 (2003).
13. Pouille, F. & Scanziani, M. Routing of spike series by dynamic circuits in the hippocampus. *Nature* 429, 717-723 (2004).
14. Traub, R.D. & Miles, R. *Neuronal networks of the Hippocampus* (Cambridge University Press, Cambridge, 1991).

Supplementary Table 1: Fraction of spikes suppressed by feedback inhibition

τ_{inh} (msec) \ g_{inh} (nS)	2	4	6
12.5	0.18	0.24	0.28
25	0.19	0.30	0.42
37.5	0.26	0.35	0.50
50	0.33	0.45	0.58

Supplementary Table 1: Fraction of spikes suppressed by feedback inhibition implemented via dynamic clamp, in PY neurons responding to non-rhythmic trains of sEPSCs (8 nS, 1000 Hz). For comparison, when feedback inhibition when implemented via optical stimulation of PV interneurons, the fraction of spikes suppressed by was 20 $\pm$ 3% (n = 4 cells). Stronger inhibitory conductances produced more extreme spike suppression (30-70%). Feedback inhibition consisted of a monoexponentially decaying conductance with the parameters shown in the table, reversed at -60 mV, and occured 2.5 msec after each PY neuron spike. n=4 cells.

Supplementary Table 2: Change in peak γ power (with inhibition - without inhibition)

τ_{inh} (msec) \ g_{inh} (nS)	2	4	6
12.5	0.12 ± 0.36	-0.16 ± 0.40	0.03 ± 0.25
25	-0.20 ± 0.12	0.33 ± 0.48	0.12 ± 0.14
37.5	0.26 ± 0.26	0.24 ± 0.13	0.19 ± 0.11
50	-0.12 ± 0.14	-0.11 ± 0.10	0.26 ± 0.18

Supplementary Table 2: Change in peak power in the γ (30-80 Hz) range. Change was calculated as the peak power when inhibition was present minus the peak power in the absence of inhibition. None of these changes were statistically significant. The effects shown in this table were calculated from the responses of PY neurons to non-rhythmic trains of sEPSCs (8 nS, 1000 Hz), when feedback inhibition was implemented via dynamic clamp. Feedback inhibition consisted of a monoexponentially decaying conductance with the parameters shown in the table, reversed at -60 mV, and occurred 2.5 msec after each PY neuron spike. For comparison, when feedback inhibition that was implemented via optical stimulation of PV interneurons, peak γ power increased by 1.30 ± 0.41 spikes^2. ± S.E.M. n=4 cells.

Supplementary Figure 1

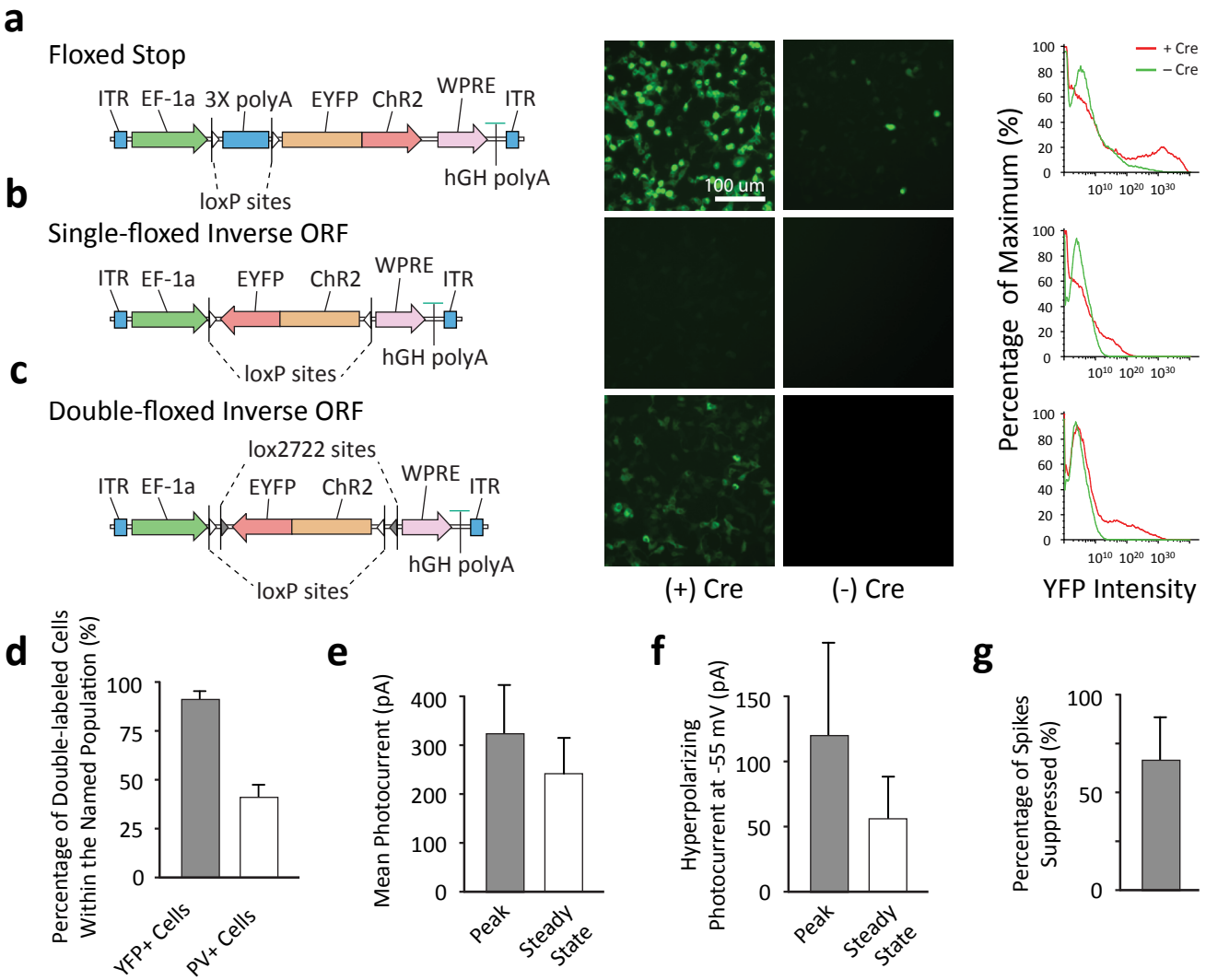

Supplementary Fig. 1. Specific targeting of PV interneurons. a, Left: Construct design for the floxed-stop strategy. Middle: floxed-stop ChR2-EYFP with and without co-transfection of Cre recombinase. Right: FACS analysis of floxed-stop ChR2-EYFP cells with (red) and without (green) cotransfection of Cre. **b,** Left: Construct design for the single-floxed inverted open reading frame (SIO) strategy. Middle: SIO:ChR2-EYFP with and without co-transfection of Cre. Right: FACS analysis of SIO:ChR2-EYFP cells with (red) and without (green) co-transfection of Cre. **c,** Left: Construct design for the double-floxed inverted open reading frame (DIO) strategy. Middle: DIO:ChR2-EYFP with and without co-transfection of Cre. Right: FACS analysis of DIO:ChR2-EYFP cells with (red) and without (green) co-transfection of Cre. Cells expressing the DIO:ChR2-EYFP construct exhibited 2.0 ± 0.1 fold more fluorescent cells with a 6.5 ± 0.6 fold higher mean relative fluorescence intensity compared to cells expressing the SIO:ChR2-EYFP construct (n = 3 sample wells for each construct). All FACS analysis was performed 24 hours after transfection and 100,000 cells were counted for each sample. **d,** Immunohistochemistry of fixed brain sections from DIO:ChR2-EYFP-injected Pvalb:Cre transgenic mice showed that 92 ± 3% of ChR2-YFP cells co-localized with parvalbumin immunoreactive cells and 41 ± 7 % of parvalbumin-immunoreactive cells also expressed ChR2-EYFP. **e,** PV ChR2-EYFP neurons exhibited mean peak and steady state photocurrents of 308 ± 97 pA and 232 ± 69 pA respectively (n = 4 cells). **f,** PV eNpHR-EYFP neurons exhibited mean peak and steady state photocurrents of 120 ± 65 and 55 ± 35 respectively (n = 3 cells; voltage clamp at -55 mV). **g,** Summary plot showing the percentage of spikes inhibited by eNpHR mediated hyperpolarization during a 7.5 second-long current ramp in PV eNpHR-EYFP neurons (n = 3 cells).

Supplementary Figure 2

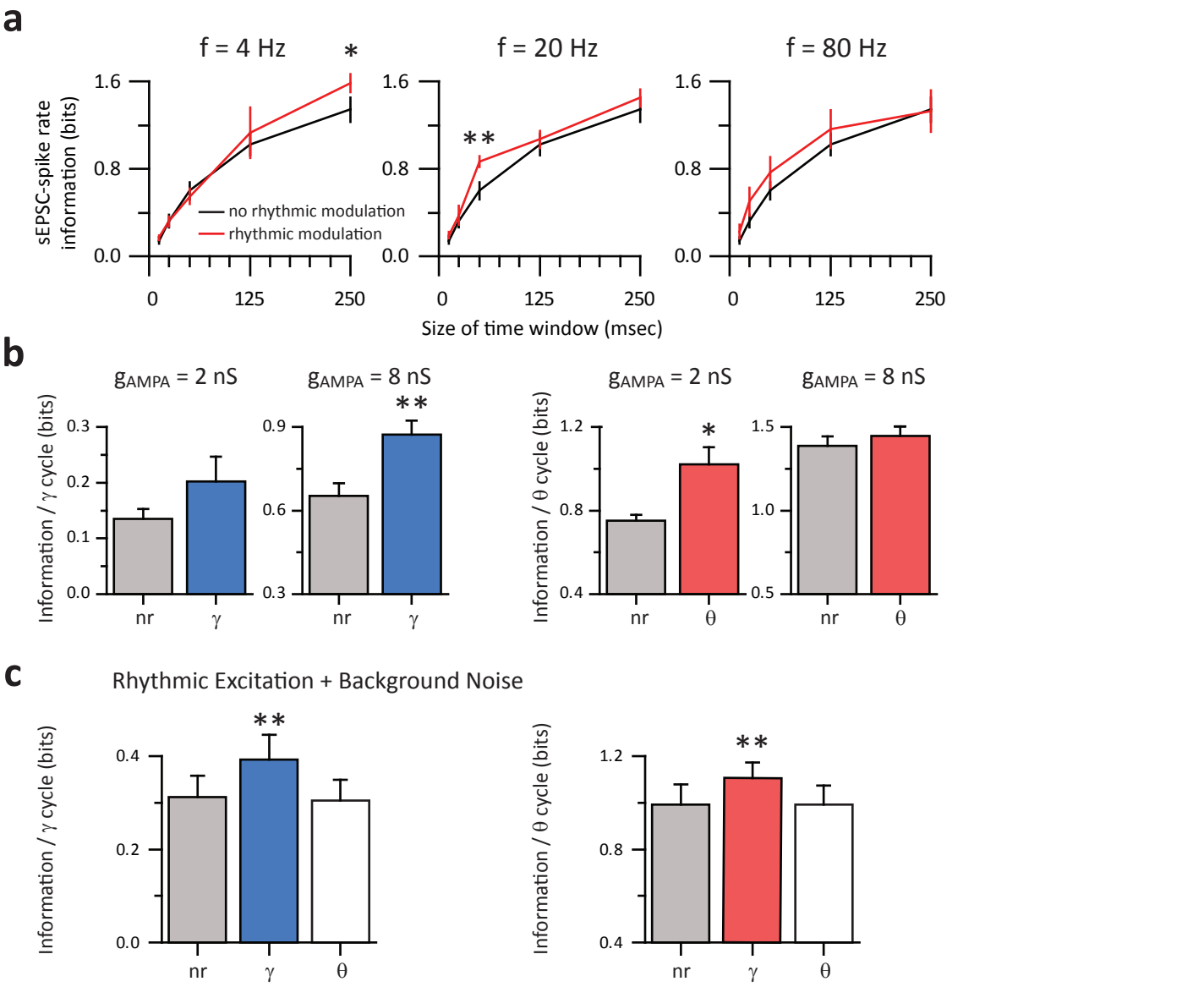

Supplementary Fig. 2. Effects of varying synaptic and input parameters on sEPSC-spike rate information. a, Dynamic clamp experiments as shown in Fig. 3, (layer V PY neurons in mPFC), modulating input at 4, 20, or 80 Hz. sEPSC-spike rate information for input modulated at various frequencies, calculated using time windows of varying sizes. In each case, we compared the information depending on whether rhythmic modulation was present (red lines) or absent (black lines), and tested for statistical significance using time windows equal to the cycle length (i.e. 250, 50, or 12.5 msec for the left, middle, and right panels, respectively). **b,** Dynamic clamp experiments using larger or smaller sEPSC amplitudes. Using a sEPSC amplitude of 2 nS, 3/6 neurons responded sparingly or not at all (e.g. average response rate < 1 Hz). In the remaining 3 neurons, θ (8 Hz) oscillations still significantly increased sEPSC-spike rate information, while there was a trend towards significance for γ (40 Hz) oscillations. When the sEPSC amplitude was 8 nS, γ oscillations continued to robustly enhance information, while there was no difference between the non-rhythmic case and θ oscillations. **c,** Additional experiments, comparing sEPSC-spike rate information in the non-rhythmic case, to rhythmic cases in which 25% of the sEPSCs occur during the trough of the oscillation, and 75% occur during the peak. In this case, the degree of sEPSC rate modulation was much smaller, but both θ and γ oscillations still significantly increased the sEPSC-spike rate information. * = $p < 0.05$, ** = $p < 0.01$, *** = $p < 0.001$. All comparisons made using two-tailed t-tests. n = 5 cells in a, 3 or 6 cells in b, and 10 cells in c.

Supplementary Figure 3

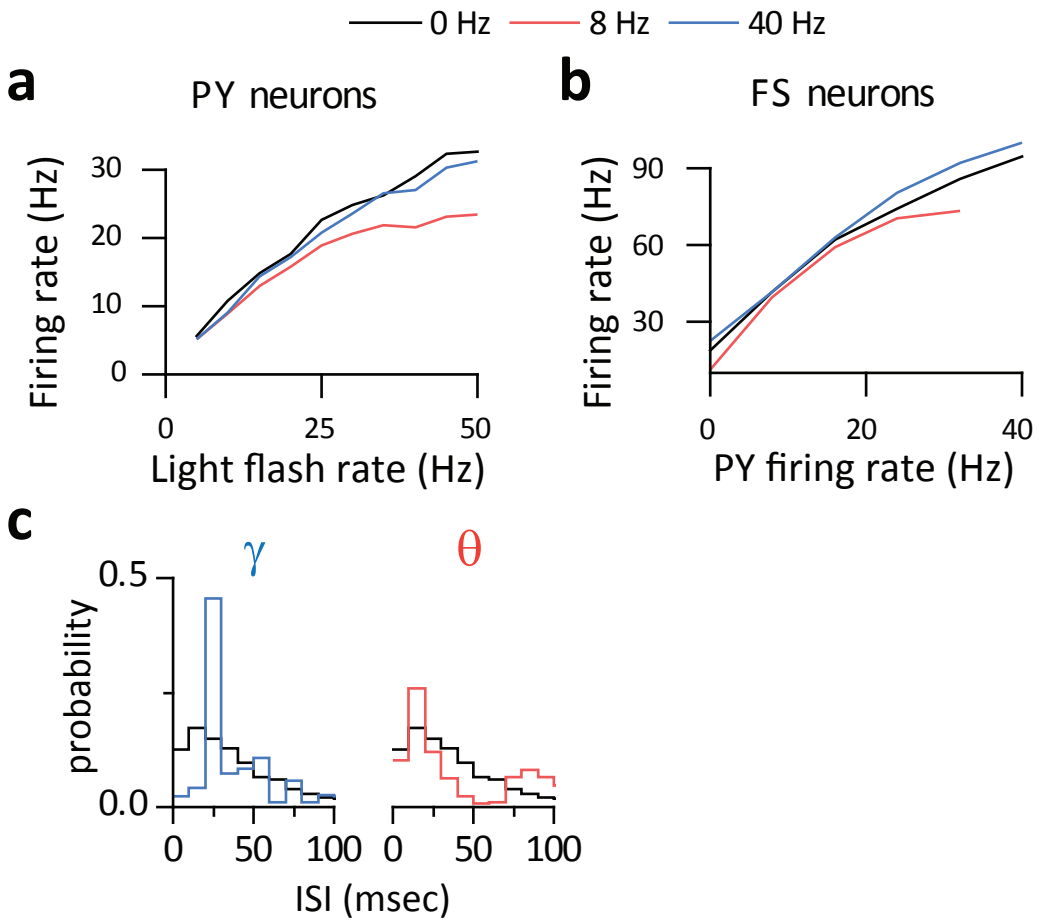

Supplementary Fig. 3. Properties of responses to light trains in pyramidal and fast-spiking neurons from Thy1 transgenic mice. **a,** shows the input-output curve for pyramidal neurons. **b,** shows the input-output curve for fast-spiking interneurons. **c,** the inter-spike interval (ISI) distribution during pyramidal neuron responses to rhythmic and non-rhythmic light flashes.

Supplementary Figure 4

a

L-ITR: 1-141
EF-1a Promoter: 156-1264
lox2722: 1450-1483
loxP: 1534-1567
Inverted ChR2-EYFP: 1579-3204
lox2722: 3251-3284
loxP: 3335-3368
WPRE: 3383-3991
hGH polyA Signal: 4011-4489
R-ITR: 4529-4669
f1 Origin: 4767-5067
AmpR Marker: 5586-6443
pUC Origin: 6594-7261

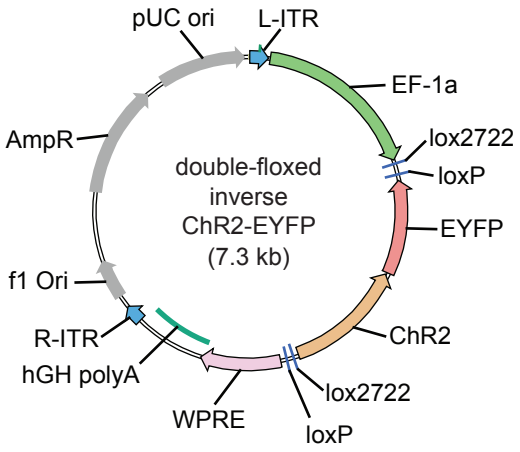

b

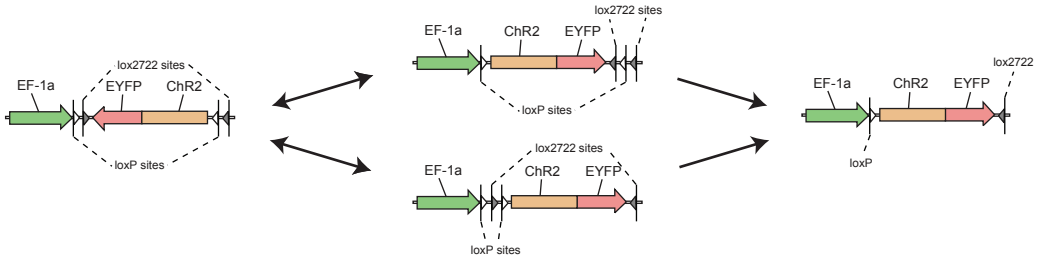

c

EF-1a

*Bam*HI *Sal*I

aggtaccggatcctctagagtcgactccggaataacttcgtataggatactttatacgaagttatgcag

*Kpn*I *Xba*I *Bsp*EI lox2722 >

aatggtagctggattgtagctgctattagcaatatgaaacctcttaataacttcgtatagcatacatta

loxP >

tacgaagttatggcgcgcc Inverted ChR2-EYFP ggtggctagcataactt

loxP > *Asc*I *Nhe*I

cgtataaagtatcctatacgaagttatttgccttaacccagaaattatcactgttattctttagaatgg

< lox2722

WPRE

tgcaaagaataacttcgtataatgtatgctatacgaagttatgaattcgatatcaag

< loxP *Eco*RI

Supplementary Fig. 4. Detailed description of vector system. **a,** Plasmid map showing the features of the double-floxed inverse ChR2-EYFP vector. **b,** Mechanism of Cre recombinase-mediated activation of the double-floxed-inverse ChR2-EYFP transgene. **c,** Sequence information for the double-floxed inverse ChR2-EYFP transgene cassette. Restriction sites suitable for cloning and lox recombination sites are shown.

Supplementary Figure 5

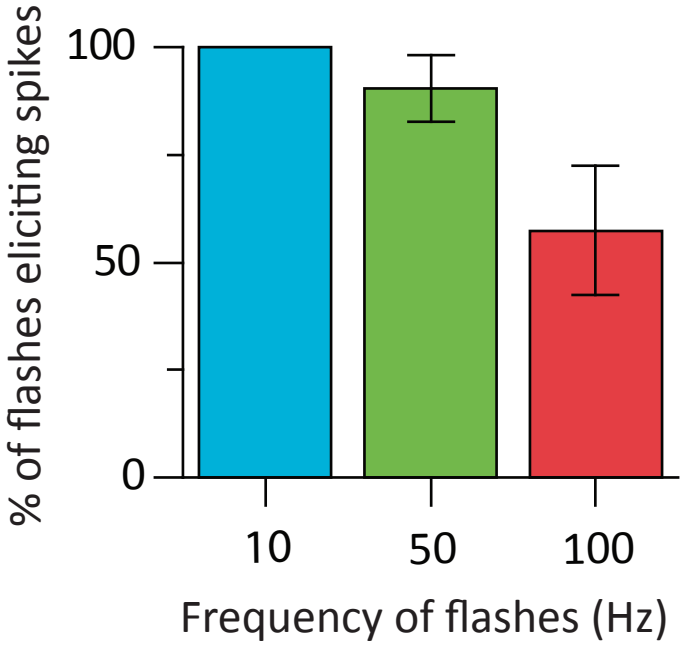

Supplementary Fig. 5. Frequency-response of pyramidal neurons in Thy1 transgenic mice. The fraction of blue light flashes (1 msec in duration) that elicited spikes during 500 msec long trains of light flashes occurring at various frequencies *in vitro*. Recordings were from layer V pyramidal neurons in the medial prefrontal cortex of transgenic mice expressing ChR2 under control of the Thy1 promoter, and under the same conditions as Fig. 4. n = 5-11 cells for each frequency.

Supplementary Figure 6

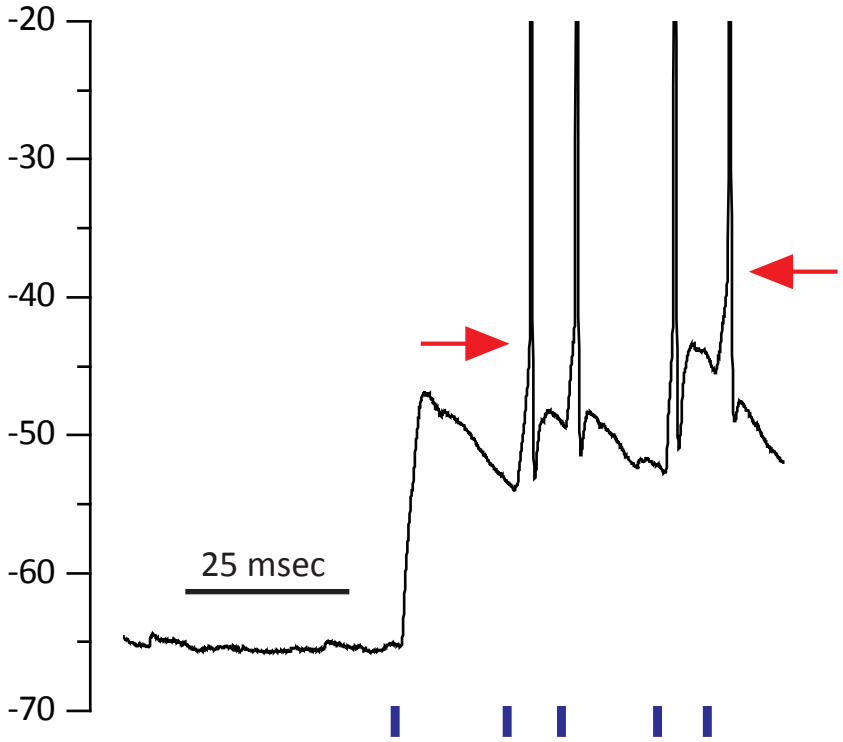

Supplementary Fig. 6. Current clamp recording from a fast-spiking interneuron in a Thy1 transgenic mouse. Responses to 1 msec long flashes of blue light in vitro are shown. The recording conditions are identical to those in Fig. 4. Red arrows indicate spike threshold. Note the long-lasting depolarization and EPSPs after light flashes.

Supplementary Figure 7

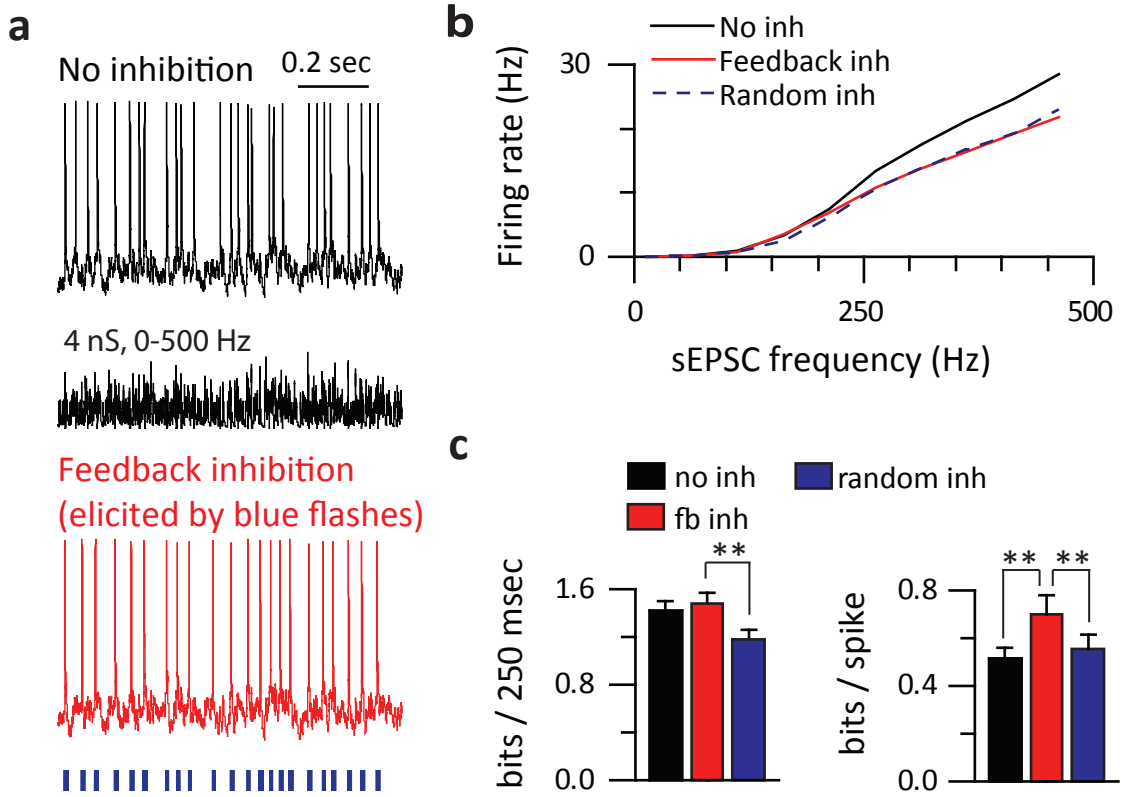

Supplementary Fig. 7. Feedback inhibition from PV interneurons suppresses redundant spikes and makes rate coding more efficient. a, Using dynamic clamp to stimulate PY neurons with sEPSC trains, and light flashes to activate PV interneurons, as illustrated in Fig. 2c, we studied the effects of feedback inhibition on sEPSC-spike rate information. These experiments used non-rhythmic trains of sEPSCs with a unitary conductance of 4 nS. As in earlier experiments (c.f. Fig. 3), the rate of sEPSCs changed every 500 msec and varied between 50 and 500 Hz. **b,** Mean firing rates of PY neurons as a function of the input sEPSC rate. Black trace: no feedback inhibition. Red trace: feedback inhibition present, i.e. PY neuron spikes trigger light flashes which activate PV interneurons. Dotted blue trace: "Random inhibition," starting with spike trains recorded in the absence of inhibition, we randomly eliminated spikes to match spike counts obtained in the presence of inhibition. Spike counts were matched for each 5 second long sweep. **c,** Left: sEPSC-spike rate information (computed using a 250 msec time window) for the three cases described above, no inhibition (black), feedback inhibition (red), and random inhibition (blue). Whereas randomly eliminating spikes markedly reduced sEPSC-spike rate information, feedback inhibition does not affect the sEPSC-spike rate, suggesting that feedback inhibition selectively suppresses redundant spikes. Right: the sEPSC-spike rate information, normalized by the mean number of spikes in each 250 msec window. n = 6 cells for panels b, c. ** = $p < 0.01$.

Supplementary Figure 8

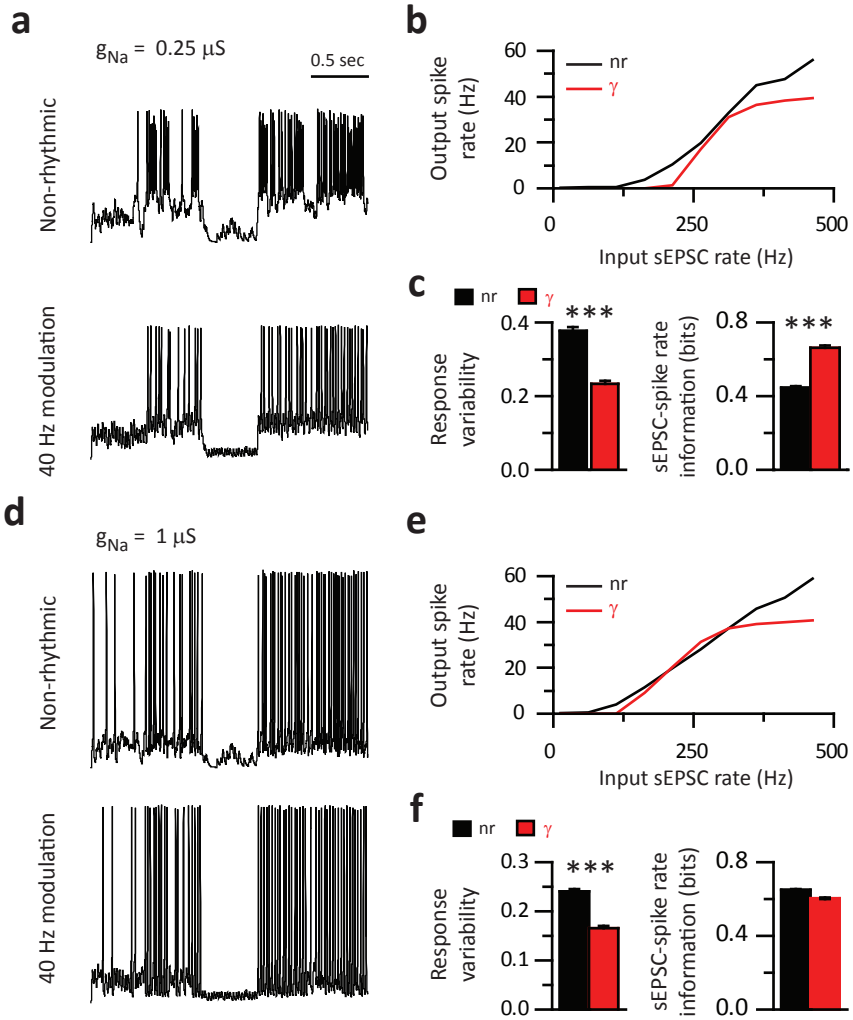

Supplementary Fig. 8. Effects of γ rhythms on sEPSC-spike rate information in biophysical model neurons. a, Simulated responses of a single-compartment biophysical model neuron to non-rhythmic (top) and γ-modulated (bottom) sEPSC trains. Same sEPSC trains as in Fig. 3. g_{Na} = 0.25 μS. **b,** The output spike rate of the same model neuron shown in a, as a function of the input sEPSC rate for non-rhythmic (black) and γ-modulated (red) sEPSC trains. **c,** Left: Population data: response variability of 10 model neurons (with distinct input resistances and resting potentials; Methods) to non-rhythmic (black) and γ-modulated (red) sEPSC trains. Right: Population data: sEPSC-spike rate information (calculated using 25 msec windows) for non-rhythmic (black) and γ-modulated (red) sEPSC trains. **d – f,** same as a-c, but for model neurons with g_{Na}= 1 μS (g_{Na}:g_K = 0.5 for both sets of simulations). Both sets of simulations generate more sigmoidal input-output (I-O) curves and decreased response variability in response to γ-modulated sEPSC trains than for non-rhythmic trains, but did not fully reproduce increased gain-response to γ-modulated sEPSC trains using these or a wide range of other parameters (Methods). Decreased response variability enhanced sEPSC-spike rate information for g_{Na} = 0.25 μS, but not for higher values of g_{Na} due to the fact that decreased response variability is counteracted by a decreased response entropy associated with leveling-off of the I-O curve at high sEPSC rates during γ-modulated trains. These data suggest that finely tuned active conductances can reproduce the effects of γ-oscillations on sEPSC spike-rate information. Similarly, γ-oscillations did not increase sEPSC-spike rate information in integrate-and-fire neurons (Fig. 3e), because as EPSCs became more concentrated in time, opportunities for spiking were reduced, and the consequent decrease in the range of spike rates outweighs reductions in spike variability. Thus, the combination of substantially increased gain and reduced noise that enhances sEPSC-spike rate information in real neurons (Fig. 3) is actually quite difficult to obtain in simple models and points to the exquisite design of the γ-modulated network and network elements. *** = $p < 0.001$.